END

FILMED

DTIC

A Beam Current Density Monitor
for Intense Electron Beams

RALPH B. FIORITO

Naval Surface Weapons Center
White Oak, Md.

MICHAEL RALEIGH

Plasma Physics Division

STEPHEN M. SELTZER

National Bureau of Standards ·
Washington, D.C.

NAVAL RESEARCH LABORATORY
Washington, D.C.

84 01 24   021

REPORT DOCUMENTATION PAGE	READ INSTRUCTIONS BEFORE COMPLETING FORM

1. REPORT NUMBER	2. GOVT ACCESSION NO.	3. RECIPIENT'S CATALOG NUMBER
NRL Memorandum Report 5241	*A137146*	

4. TITLE (and Subtitle)	5. TYPE OF REPORT & PERIOD COVERED
A BEAM CURRENT DENSITY MONITOR FOR INTENSE ELECTRON BEAMS	Interim report on a continuing problem
	6. PERFORMING ORG. REPORT NUMBER

7. AUTHOR(s)	8. CONTRACT OR GRANT NUMBER(s)
Ralph B. Fiorito,* Michael Raleigh, and Stephen M. Seltzer**	

9. PERFORMING ORGANIZATION NAME AND ADDRESS	10. PROGRAM ELEMENT, PROJECT, TASK AREA & WORK UNIT NUMBERS
Naval Research Laboratory Washington, DC 20375	61153N:RR011-09-41; 47-0871-03 62707;0;0R40AA; 47-0922-03

11. CONTROLLING OFFICE NAME AND ADDRESS	12. REPORT DATE
Office of Naval Research, Arlington, VA 22217	December 28, 1983
Defense Advanced Research Projects Agency	13. NUMBER OF PAGES
Arlington, VA 22209 (Con't)	20

14. MONITORING AGENCY NAME & ADDRESS(if different from Controlling Office)	15. SECURITY CLASS. (of this report)
Naval Surface Weapons Center	UNCLASSIFIED
White Oak, MD 20910 - Attn: R-401	15a. DECLASSIFICATION/DOWNGRADING SCHEDULE

16. DISTRIBUTION STATEMENT (of this Report)

Approved for public release; distribution unlimited.

17. DISTRIBUTION STATEMENT (of the abstract entered in Block 20, if different from Report)

18. SUPPLEMENTARY NOTES

*Naval Surface Weapons Center, White Oak, MD
**National Bureau of Standards, Washington, DC
(Con't)

19. KEY WORDS (Continue on reverse side if necessary and identify by block number)

Electron Beam
Current Monitor
Current Density

20. ABSTRACT (Continue on reverse side if necessary and identify by block number)

We describe a new type of interceptive electric probe for mapping the radial current density profile of high energy (>4 MeV), high current (>1 kA) electron beams.

DD $\substack{\text{FORM} \\ 1 \text{ JAN } 73}$ 1473   EDITION OF 1 NOV 65 IS OBSOLETE
S/N 0102-014-6601

11. CONTROLLING OFFICE NAME AND ADDRESS (Continued)

Naval Seas Systems Command (PMS 405), Arlington, VA 20360

18. SUPPLEMENTARY NOTES (Continued)

Research supported by the Office of Naval Research and by the Defense Advanced Research Projects Agency (DoD) ARPA Order No. 4395 Amendment 11 monitored by the Naval Surface Weapons Center under Contract N60921-83 WR-W0114.

CONTENTS

A BEAM CURRENT DENSITY MONITOR
FOR INTENSE ELECTRON BEAMS

I. INTRODUCTION

→ *The authors*

~~We describe~~ a new type of ~~electric~~ probe for mapping the radial current density profile of high-energy (>4 MeV), high-current (>1 kA) electron beams. The idea of developing an electrically sensitive probe for these conditions was originally suggested to one of the authors (R. Fiorito) during a years visit to the Lawrence Livermore National Laboratory (LLNL). The resulting probe is intended for use on the Experimental Test Accelerator (ETA) and the Advanced Test Accelerator (ATA) at that laboratory.

In a preliminary experiment, a bare wire probe was inserted in the ETA beam. The dominant signal from this probe was due to a capacitive coupling between the entire beam and the probe. (The probe also rang at ~500 kHz.) In order to alleviate these problems, a new probe was designed which incorporated an electrostatic shield (Fig. 1). The sensing tip and supporting stalk of the probe now form an open-ended, but shielded, 50 Ω coaxial line. The outer conductor of the line constitutes the electrostatic shield. Tests at the Naval Surface Weapons Center (NSWC) using a Febetron 705X generator (1 − 2 MeV) confirmed the shielding effect.

The probe is inserted radially into the electron beam from the beam line wall (Fig. 2). The beam passes through the probe and secondary electrons "knocked on" from the tip result in a signal proportional to the intercepted current. A small electrostatic coupling to the beam charge present inside the tip and between the tip and the shield gives an additional signal proportional to the time derivative of the intercepted current. The shielded probe possesses the spatial resolution to allow the beam profile to be determined by mechanically scanning the probe through the beam as a function of radius.

Because of their repetitive nature, the ETA and ATA beams will cause substantial heating of the probe. Experience by the LLNL group with other probes dictated that the sensing tip should be made of graphite in order to survive. As a result of tests at the Naval Research Laboratory (NRL), a probe construction was found that would tolerate the expected temperatures.

This *discusses*

~~In the~~ report ~~that follows we discuss~~ in detail: the mechanical design, the electrical response, and temperature effects, as they pertain to the electric probe, and describe the first experimental results obtained using this probe on ETA.

II. MECHANICAL DESIGN

Figure 3 shows a detailed diagram of the probe built at NRL and subsequently used on ETA. The major parts of the probe are: (1) the inner tip made of AXFQ-50 Poco graphite, (2) a 304 stainless steel support which holds the sensing tip and forms its electrical connection, (3) the electrostatic shield, also made of Poco graphite, (4) a nosepiece which holds the outer tip, (5) a 3/4" O.D. stainless steel tube into which the nosepiece is pressed, (6) a teflon plug which both holds the inner conductor and forms a vacuum seal, and (7) a pump-out hole.

The entire probe, both the graphite sensing tip and the stainless steel stalk, is designed to closely approximate a "capped-off" 50 Ω coaxial transmission line i.e. an open ended but shielded line. The inner tip is 1 mm in diameter. The electrostatic shield is 2.3 mm I.D. with 1 mm walls. The length of the sensing tip is 6 cm.

The graphite parts of the probe couple to their stainless steel supports via interference fit joints. The joints are expected from thermal calculations (see section VII) to operate at ~500 K. Differential expansion causes the joints to become loose at ~1000 K. The wall thickness of the stainless steel sleeves is such that at room temperature the compressive stress caused by the sleeves is less than the yield stress of the graphite. The neck just behind each joint can be bent to adjust the alignment of the probe.

The pump-out hole in the nosepiece allows the probe to be evacuated by the beam-line vacuum. This prevents the probe from being shorted by an internal plasma. The probe vacuum could also be provided externally which would allow the probe to operate in a gas filled beam line.

The probe is assembled in the following order: (1) press the inner conductor into the teflon plug, (2) press that assembly into the stainless steel pipe, (3) press a 1/4" diameter graphite blank into the inner conductor, (4) turn the blank to final size in one pass using a follow rest, (5) correct the alignment of the center conductor, if necessary, by bending the neck, (6) press a pre-drilled graphite blank into the nosepiece, (7) press the nosepiece into the stainless tube, (8) correct the alignment of the outer blank, if necessary, (9) turn the outer blank to size using a follow rest, (10) x-ray the probe from two orthogonal angles to check the internal alignment (Fig. 4), and (11) bend the neck in the nosepiece, if necessary, to correct the internal alignment.

III. CONDUCTION CURRENT SIGNALS

The incident beam produces a conduction current signal, which is proportional to the rate of electron deposition/depletion in the sensing tip. Because the radius of the probe represents a small fraction of the range of electrons above a few MeV, the incident primary electrons pass through the probe. Electron deposition in the sensing tip is due to secondary, knock-on electrons whose tracks begin in the electrostatic shield and end in the core. Electron depletion in the tip is due to secondaries whose tracks begin in the tip and end outside it. As will be seen, the latter dominates in the cases considered here, and the result is a net electron depletion.

Calculations of this deposition/depletion were done with the cylindrical version of the Monte Carlo code ETRAN.[1] Because this version of the code treats only homogenous targets, the gap between the shield and the tip could not be properly taken into account. Instead, two target representations (Fig. 5) were considered which should set limits for the net electron depletion. In case a), the gap was neglected and the probe assumed to be a solid graphite cylinder of 1.5 mm radius with a central core region, the sensing tip, of 0.5 mm radius. Neglecting the gap will lead to an underestimate of the electron depletion in that all secondaries crossing inward from the shield must now enter the tip to possibly stop there. In case b), the probe was assumed to consist of the core alone, i.e. just the bare sensing tip. In this case the electron depletion will be greatly overestimated due to the complete neglect of secondaries crossing inward from the shield.

In both cases a uniform electron flux was assumed incident everywhere along a long (~100 mm) cylinder so as to minimize any end effects. Calculations were initially done for 5 MeV and 50 MeV incident electrons, based, in each case, on samples of 50,000 primary histories and all secondaries produced with energies greater than 10 keV. The range in graphite of electrons with energies below 10 keV is less than 0.0016 mm. This is very small compared to the dimensions of the probe and justifies this choice of the cut-off energy.

The results are given in Table 1 in terms of an electron deposition coefficient A, defined as the number of electrons deposited per unit length of probe in the beam, per unit incident electron flux. When the coefficient A, which has units of length, is multiplied by the length of the probe in the beam, l, and by the average incident current density,* the result is the signal current which flows from the probe:

$$I_{signal} = Al <j> \quad \text{(amps)}. \tag{1}$$

$*<j> = \frac{1}{l} \int_0^l j\,dr$

2

Table 1 — Electron-Deposition Coefficient A
in Units of cm

Electron Beam Energy (MeV)	Shielded Core	Bare Core
5	-1.32×10^{-3}	-4.77×10^{-3}
50	-1.40×10^{-3}	-4.94×10^{-3}

A is negative for the 5- and 50-MeV energies and for both the shielded-core and bare-core geometries, indicating a net electron depletion in all cases. The bare-core results are nearly four times larger in magnitude than those for the shielded core, so that only rather wide limits would appear to have been set for the actual probe. However, because the shielded-core geometry is much closer to that of the actual probe, the shielded-core results are expected to be more applicable.

Calculations were then done at several other energies for the shielded-core geometry. The results of these calculations are plotted in Fig. 6. Above ~4 MeV an apparently small energy dependence of the results is difficult to separate from statistical fluctuations inherent in the Monte Carlo calculations. Based on the curve in Fig. 6, the conduction current can be expected to be only slightly larger for 50 MeV electrons in the ATA as for 5 MeV electrons in the ETA, and results for electrons with even higher energies can be estimated by extrapolation.

IV. DISPLACEMENT CURRENT SIGNALS

The presence of beam charge within the probe will cause displacement currents to flow in the tip and the shield. We consider this process in several steps (Fig. 7). In Step a), we have made an instantaneous introduction of beam charges. (For an electron beam $Q_1, Q_2,$ and $Q_3,$ are negative numbers). The conduction electrons in both the tip and the shield will adjust on an electrostatic time scale (or at the speed of light, whichever is slower) to produce the surface charges shown in b). Current then flows from the tip to the shield until they reach a common potential as shown in c). This balanced flow accompanies the transverse mode of the coax. The common mode is assumed to be blocked by the ground loop inductance. The enclosed charges Q_1, Q_2, and Q_3, have now been effectively transported to the outer skin of the probe. They will drain down the outer skin to the beam-line wall, whereupon the common potential will be the beam line wall potential.

We designate the surface charge on the tip as $-k_i Q_2$. The electric field between the conductors then follows from Gauss' law (neglecting end effects)

$$E(r) = \frac{\sigma}{2\pi\epsilon r}\left[k_i - \frac{(r^2 - r_i^2)}{r_o^2 - r_i^2}\right] \tag{2}$$

where σ is the charge per unit length $(\sigma = Q_2/l),$[**] and r_i and r_0 are the radii of the sensing tip and the inside surface of the electrostatic shield, respectively. When the conductors reach common potential we have

$$\int_{r_i}^{r_o} E \cdot dr = 0. \tag{3}$$

Substituting for $E(r)$ we find

$$k_i = \frac{(r_o^2 - r_i^2) - 2r_i^2 \ln(r_o/r_i)}{2\ln(r_o/r_i)(r_o^2 - r_i^2)}. \tag{4}$$

[**]MKS units will be used for the equations in sections IV and VI.

3

Thus the total charge that flows from the tip is given by

$$\Delta Q = Q_1 + k_i Q_2. \tag{5}$$

The displacement current which flows in the probe will be the time derivative of this displaced charge. The displacement signal is therefore given by

$$I_{\text{signal}} = \frac{\partial}{\partial t} (Q_1 + k_i Q_2). \tag{6}$$

In analogy to Eq. 1 we may define a coefficient B such that

$$I_{\text{signal}} = Bl < \partial j / \partial t >, \tag{7}$$

where $j = -n_e ec$ is the beam current density. It follows from Eq. 4 that

$$B = \frac{\pi}{c} \left\{ r_i^2 + (r_o^2 - r_i^2) k_i \right\}. \tag{8}$$

The numerical value of B is 6.4×10^{-13} (cm. sec.).

V. RESPONSE TIME

The response time of the probe is the combined effect of the transit time of the beam across the probe, the electrostatic relaxation time, dispersion in the graphite coax, and transit times for reflections from the open end of the line. The beam transit time is

$$t = 2 \frac{r_{\text{probe}}}{c} \approx 10^{-11} \text{ sec.}$$

The electrostatic relaxation time is

$$t = \frac{\epsilon}{\sigma} \approx 10^{-16} \text{ sec.}$$

The dispersion in the graphite coax was determined experimentally using a time domain reflectometer (TDR). The TDR was connected to a complete probe (Fig. 8a) and to a probe with the graphite tip missing (Fig. 8b). The rise time of the reflected TDR pulse differed slightly in the two cases. The difference implied a rise time of $\sim 5 \times 10^{-11}$ sec. for a single pass through the graphite coax.

The probe is fundamentally very fast as seen above. The primary response time limitation results from the open ended configuration. Imagine that signal pulses are generated in the coaxial probe approximately one beam radius from the open end. The time delay between receipt of the first pulse and the reflection is then

$$t = \frac{2r_b}{c},$$

which is $\sim 10^{-10}$ sec for $r_b \sim 1$ cm.

VI. ELECTROSTATIC SHIELDING

The probe inside the beam line constitutes a 1/4 wave stub with a resonant frequency of ~ 1 GHz. The sudden introduction of the beam will excite this resonance (as was in fact observed with the unshielded probe mentioned in the introduction). The probe will also be subject to RF fields due to noise on the beam (e.g. the beam breakup instability in ETA at ~ 800 MHz). For the shielding to be effective the excited current flows must be restricted to a depth which is small compared to the shield thickness. The skin depth is given by[2]

4

$$\delta = \frac{1}{\sqrt{\pi f \mu \sigma}}, \tag{9}$$

and for graphite at ~ 1 GHz

$$\delta = 1.5 \times 10^{-5} \, m.$$

Shielding against such frequencies is therefore excellent. For applied fields of significantly lower frequency the forced current flow simply keeps the probe grounded to the beam line wall.

VII. PROBE HEATING

An equilibrium temperature, T_{eq}, for the probe tip can be calculated by balancing the average input power, $\bar{P}_{in}$, from the beam with the radiated output power, $\bar{P}_{out}$ (in this particular case the ripple in T_{eq} is small). The input power is given by

$$\bar{P}_{in} = \frac{\tau_{pulse}}{\tau_{rep}} \, \rho \left| \frac{\partial E}{\partial(\rho x)} \right| \frac{I_b V}{\pi r_b^2 e}, \tag{10}$$

where V is the immersed volume of the probe tip and is given by

$$V = 2r_b \, \pi r_p^2 \tag{11}$$

for a fully inserted probe, where r_p is the outer radius of the electrostatic shield. The output power is given by

$$\bar{P}_{out} \approx \sigma T^4 2r_b \cdot 2\pi r_p, \tag{12}$$

where σ is the Stephan-Boltzmann constant. Equating $\bar{P}_{in}$ to $\bar{P}_{out}$ and taking

$$\tau_{rep} = 1 \text{ pps}$$
$$\tau_{pulse} = 50 \times 10^{-9} \text{ s}$$
$$\rho = 1.8 \text{ gcm}^{-3}$$
$$\frac{\partial E}{\partial(\rho x)} = 1.76 \text{ MeV cm}^2\text{g}^{-1}$$
$$I_b = 10^4 A.$$
$$r_b = 1 \text{ cm}$$
$$r_p = 2.15 \text{ mm,}$$

we obtain

$$T_{eq} \approx 1800\,^\circ \text{K} \cdot$$

This calculation can be recast to produce a limiting value for the current density. To determine this limiting value we let $T = 3800\,^\circ$K, the sublimation point of carbon. The equation for j_{limit} is

$$j_{limit} = \frac{1.3 I_b}{\pi r_b^2} = \frac{8\sigma e}{r_p} \frac{\tau_{rep}}{\tau_p} \left[\frac{\rho \partial E}{\partial(\rho x)} \right]^{-1} \cdot T^4. \tag{13}$$

Here the numerical factor 1.3 is included to account for a more realistic density profile by using a Bennett profile current density distribution. The result may be stated in terms of a maximum average current density

$$j_{avg} = j_{lim} \frac{\tau_{pulse}}{\tau_{rep}} = 4.5 \times 10^{-3} (A/\text{cm}^2).$$

5

The following model is used to calculate the temperature along the probe as a function of distance from the tip. The portion of the probe which is inserted in the beam is treated as a heat source maintained at the temperature calculated above. The remainder of the carbon probe (5.6 cm) and the stainless tube back to the vacuum seal (15 cm) is replaced by a length of carbon rod of equivalent thermal conductivity (12.4 cm). A room temperature heat sink is assumed to exist at the vacuum seal.

The heat flow down the shaft is assumed to be one dimensional, i.e., the temperature is assumed to be constant over any cross section of the probe. The differential equation for the temperature as a function of distance along the probe is determined by equating the power radiated from the edge of a slice of thickness dz to the net conductive influx:

$$\frac{d^2 T}{dz^2} = - K T^4,$$ (14)

where

$$K = \frac{2\sigma}{r\alpha},$$ (15)

and

α = thermal conductivity

r = radius

Since it is desired that the solution to Eq. (14) match the source and sink temperatures at a specified separation in z, we introduce a scaling factor, β, on z:

$$\frac{d^2 T}{dz'^2} = \frac{K}{\beta^2} T^4,$$ (16)

where

$$z' = \beta z.$$ (17)

An analytic solution exists to Eq. (16):

$$T(z') = \left[\frac{10\beta^2}{9K}\right]^{1/3} z'^{-2/3}.$$ (18)

Equation (18) may be inverted to express $z'(T)$:

$$z' = \left[\frac{10\beta^2}{9K}\right]^{1/2} T^{-3/2}.$$ (19)

The proper β may be determined by making the difference in position for the hot and cold temperatures (T_h, T_c) equal to the length of the carbon rod,

$$l = z(T_c) - z(T_h) = \left[\frac{10\beta^2}{9K}\right]^{1/2} (T_c^{-3/2} - T_h^{-3/2}).$$ (20)

Solving for β gives

$$\beta = \frac{l}{(T_c^{-3/2} - T_h^{-3/2})} \left[\frac{9K}{10}\right]^{1/2}.$$ (21)

The solution for $T(z)$ (Eq. 18 using the β given by Eq. 21) in this particular instance is shown in Fig. 9. The joint would be at the position $z \approx 6$ cm where the temperature is $\sim 500°$K.

The limits of applicability for the one dimensional model are determined by requiring that any cross section be approximately an isotherm. This is assured provided

$$\left|\frac{\partial T}{\partial z}\right| > \left|\frac{\partial T}{\partial r}\right| \text{ for all } r.$$

At the skin of the carbon rod

$$-\alpha\frac{\partial T}{\partial r} = \sigma T^4, \tag{22}$$

so we require

$$\left|\frac{\partial T}{\partial z}\right| > \frac{\sigma}{\alpha} T^4. \tag{23}$$

By expressing T and $\partial T/\partial z$ using (18) we find

$$T < \left[\frac{.4K\alpha^2}{\beta^2\sigma^2}\right]^{1/3}. \tag{24}$$

In this case the approximation is good for $T \leqslant 10,000°$K.

The thermionic emission[3] from graphite at $1800°$K is $\sim 10^{-4}$ A/cm^2. This is insufficient to produce any appreciable signal in the probe.

VIII. EXPERIMENTAL RESULTS AND DISCUSSION

The probe was tested at the Lawrence Livermore National Laboratory's Experimental Test Accelerator which is capable of producing a repetitive 4.5 MeV, 10-kA electron beam with a pulse of 25 ns FWHM. The probe was placed in the beam line immediately following the accelerator. A "beam bug"† located a few centimeters upstream from the probe location measured the total beam current as a function of time. The electric probe was radially positioned with a standard LLNL drive mechanism. This mechanism was capable of positioning the probe tip ~ 1 cm past the center of the beam line. The probe could be remotely scanned while the beam was repetitively pulsed at 1 pulse/second. A computer data acquisition system recorded probe signals and probe positions throughout the scan. Approximately 300 signal pulses per scan were accumulated.

At the same position on the beam line, but orthogonal to the electric probe, a LLNL x-ray "wire" probe consisting of a graphite tube filled with tungsten powder could also be radially scanned through the beam. This probe was approximately the same length and diameter as the electric probe. X-ray signals proportional to the intercepted current were monitored by a collimated photomultiplier tube and scan data were acquired with the same computer system as used with the electric probe.

Figure 10 shows several typical signals from the electric probe when its tip was fixed at the approximate beam centerline. Figure 11 shows the total beam current as sensed by the "beam bug". Also shown in Fig. 11 is the expected probe signal based on the theoretical values of A and B (see sections III and IV) and the "beam bug" trace. This expected signal is given by

$$V_p = 50A\int_0^{r_0} jdr + 50B\frac{\partial}{\partial t}\left[\int_0^{r_0} jdr\right]$$
$$\propto AI_{\text{beam}} + B\dot{I}_{\text{beam}}. \tag{25}$$

---

†A resistive wall current monitor.

Comparing Fig. 10 to Fig. 11 it is apparent that the probe signal contains the expected conduction current contribution but that spurious displacement effects are present. These spurious signals are attributable to motion of the electron beam centroid. This motion was known to be present, especially near the head and tail of the pulses. Such centroid motion can give large and sudden changes in the intercepted current.

Figure 12 shows scan data for the electric probe at a time of 28 ns into the pulse. The beam current is not changing at this time (Fig. 11), and the beam appears to not be sweeping laterally (Fig. 10); thus these signals may be attributed solely to the conduction current effect. The available scanning distance was insufficient for the probe to traverse the entire beam. (A full traverse of the beam would produce a sigmoid curve.) This prevents any direct determination of the beam centerline position and an experimental determination of the coefficient A. A plot of the derivative of the scan data nevertheless gives one wing of the beam profile (Fig. 13).

The theoretical value for A may be used to predict the centerline location. Using the definition of A as given by Eq. 1 we may write

$$V_p(r,t) = 50A \int_r^{r_0} j(r',t)\,dr',$$ (26)

where r is the distance to the probe tip from the center of the beam line. Taking the derivative of Eq. (26) with respect to r yields

$$\frac{\partial V_p}{\partial r} = -50Aj,$$ (27)

from which

$$j = -\frac{1}{50A}\frac{\partial V_p}{dr}.$$ (28)

The total beam current however is given by

$$I_b(t) = 2\pi \int_0^{r_0} j(r,t)\,r\,dr.$$ (29)

Substituting for j in Eq. (29) and integrating by parts leads to

$$\frac{25AI_b(t)}{\pi} = \int_0^{r_0} V_p(r,t)\,dr.$$ (30)

Assuming A and I_b are known, the centerline may be positioned so as to give the proper value to the integral in Eq. (30). The centerline in Fig. 13 was obtained in this manner. The vertical scale in Fig. 13 may also be calibrated if A is known. A measured slope of $\partial V_p/\partial r$ (V/cm), as determined for a particular position from Fig. 12, corresponds to a current density of

$$j = -\frac{1}{50A}\frac{\partial V_p}{\partial r}\,(A/cm^2)$$

according to Eq. (27).

The beam radius of 3.25 cm (HWHM), predicted by the above method, is consistent with beam transport code results for this location in the beam line.

A scan was also produced of the probe voltage numerically integrated over time (Fig. 14). This procedure removes all displacement effects of whatever origin and results in a time integrated beam profile (Fig. 15). The beam centerline and the vertical scale were determined by methods analogous to those used above.

8

The time integrated scan results in a narrower profile (2.45 cm HWHM) than the time resolved result. This implies that the radius of the beam was largest during times of maximum current.

The scan curve from the x-ray probe, numerically integrated over time, is shown in Fig. 16. The ordinates for each scan curve are scaled so as to match at the final probe position. When this is done both curves are seen to have identical shapes (Fig. 14). We believe therefore that the beam was cylindrically symmetric even though it wandered from the axis of the beam line and that both types of probe are capable of accurately profiling the beam.

IX. CONCLUSIONS

The concept of a simple electric probe for measuring current density in an intense relativistic electron beam has been successfully demonstrated. As a result of the experiments performed with this probe we conclude that (1) the theoretical analysis presented here is basically correct, (2) the probe is sensitive to beam sweep, but it can profile $j(r,t)$ whenever the beam is quiescent and can profile $\int j(r,t)\,dt$ under any conditions, and (3) a survivable probe can be constructed.

The advantages of the electric probe are (1) it is relatively cheap and easy to reproduce, (2) it fits within an o.d. of 0.75 in., (3) it has very fast time response ($\sim 10^{-10}$ sec), and (4) it produces an electric signal directly, and the signal is proportional to the intercepted electron beam current. The disadvantages are (1) it must be inserted into the electron beam, (2) in order to obtain a profile, the probe must be scanned through a repetitive, reproducible beam, and (3) it has limited spatial resolution, ~ 2.5 mm.

X. ACKNOWLEDGMENTS

REFERENCES

1. M.J. Berger and S.M. Seltzer, NBS Reports: 9836 and 9837 (1968); see also Oak Ridge National Laboratory, Radiation Shielding Info. Rep. CCC-107.

2. S. Ramo, J.R. Whinnery, and T. Van Duzer, *Fields and Waves in Communication Electronics*, John Wiley and Sons Inc., New York 1967, p. 252.

3. V. Hughes and H. Schultz, *Atomic and Electron Physics, Part A*, Academic Press, New York, 1967, p. 6.
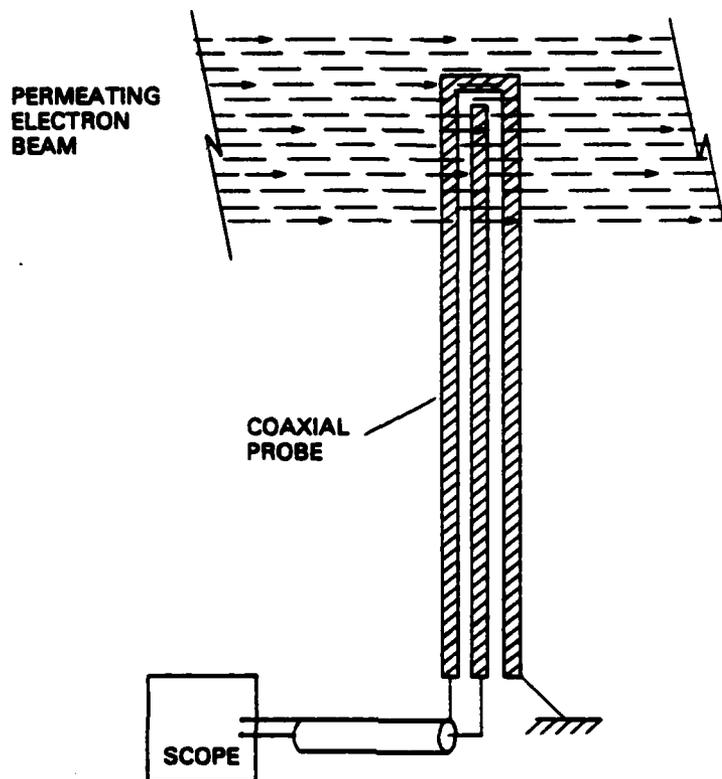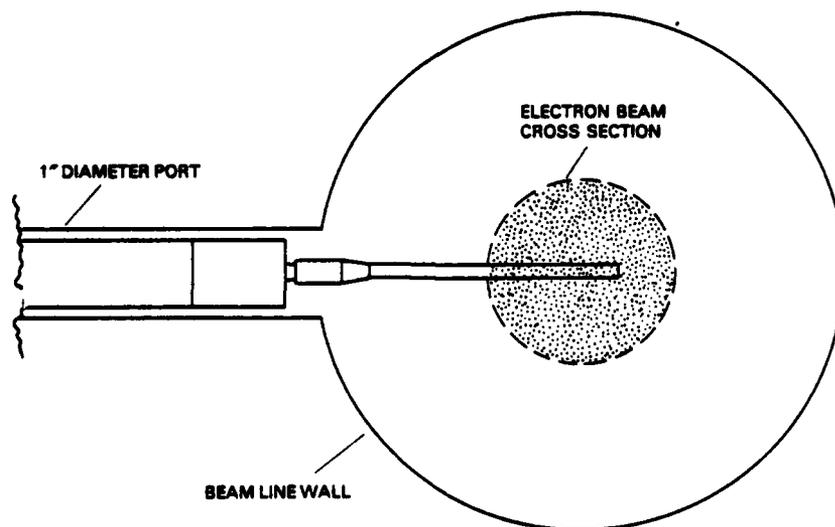
Fig. 1 — A simplified diagram of the probe

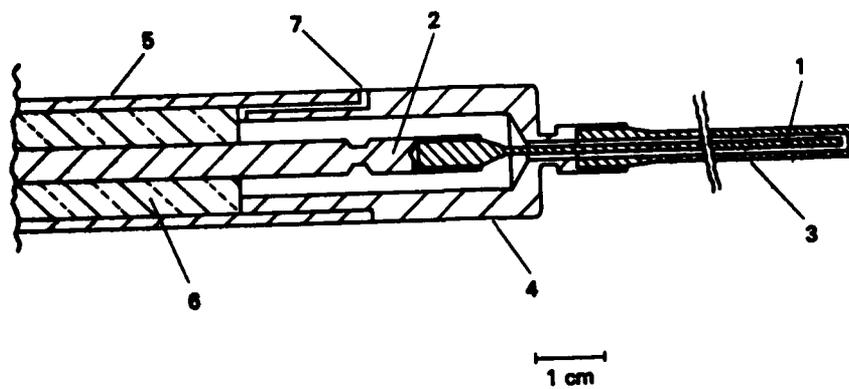Fig. 2 — The deployment of the probe within the beam line

10

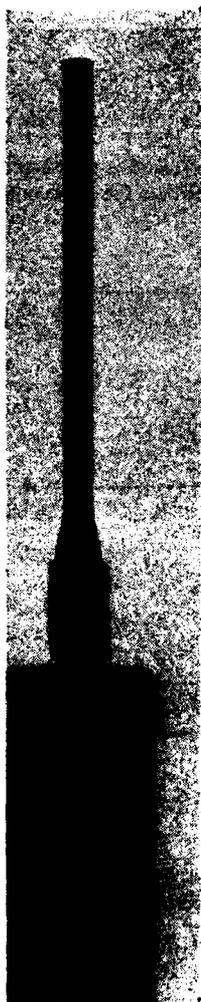Fig. 3 — A detailed diagram of the head of the probe. The components are described in the text.

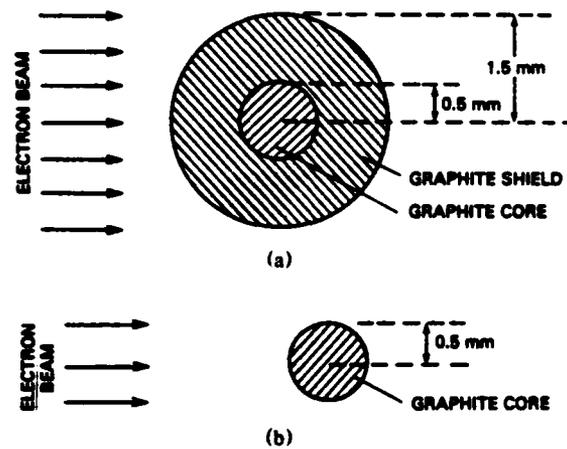Fig. 4 — An x-ray photograph of the head of the probe

11

Fig. 5 — Two representations of the probe cross section
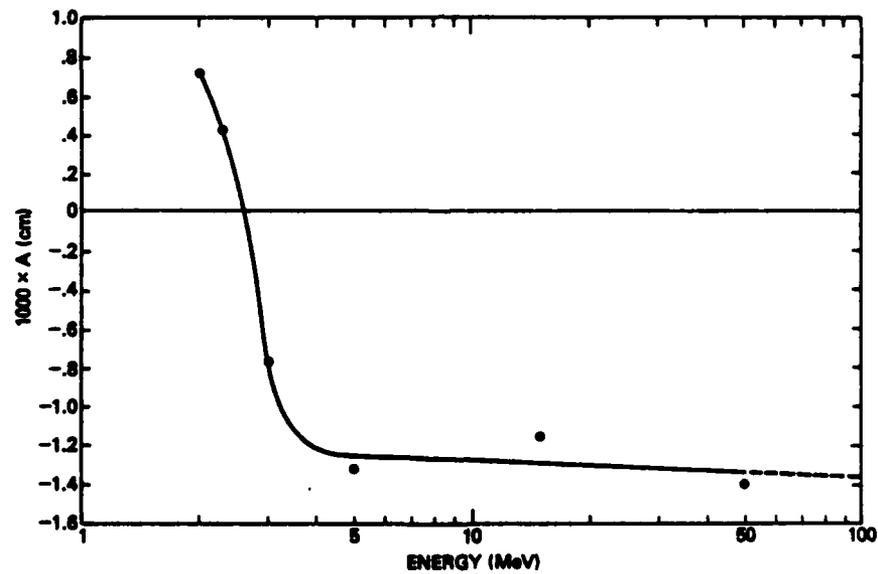which are used to calculate the conduction current signals

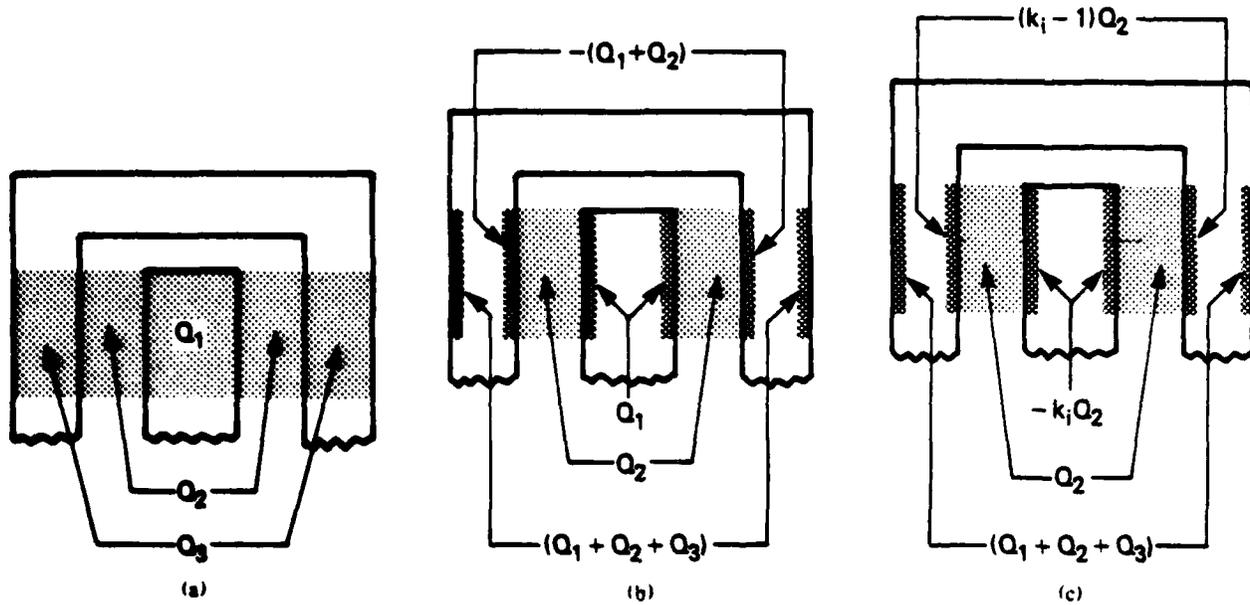Fig. 6 — The electron deposition coefficient, A, versus energy for
the shielded-core geometry

12

Fig. 7 — The re-arrangement of charge within the probe in response to beam charges transiting the probe. (a) The beam is "instantly" turned on and kept on. Q_1, Q_2 and Q_3 are the beam charges before the probe begins to respond. The probe is treated as totally transparent. There is no beam stoppage and no "knock-on." (b) A rapid electrostatic relaxation has taken place. Conduction electrons within the probe have displaced radially to produce surface charges and to eliminate the electric fields within the conductors. (c) Axial current flow has transported charge from the inner conductor to the outer conductor to bring them to a common potential.
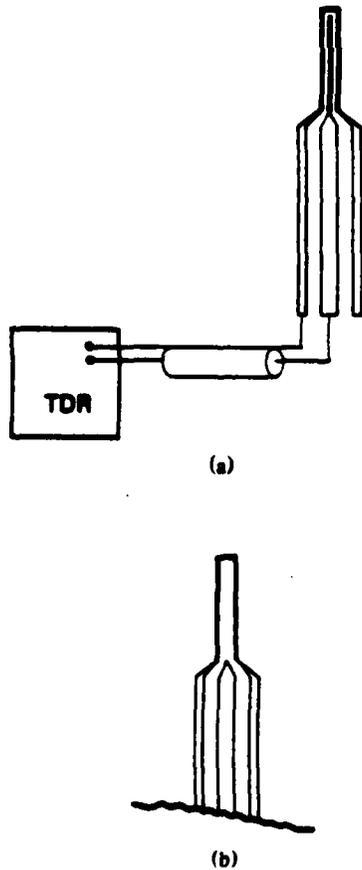
Fig. 8 — (a) The Time Domain Reflectometer (TDR) connected to a complete probe. (b) A probe from which the graphite sensing tip is missing.

13
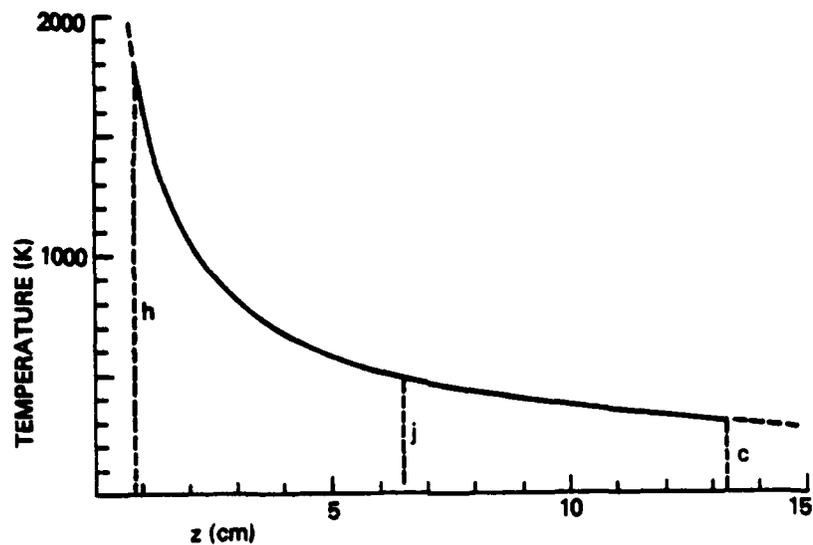
Fig. 9 — The temperature profile along the probe. The heat source is at
h, the cold sink is at c, and the graphite—stainless joint is at j.

Fig. 10 — Three typical probe signals
with the probe halfway across the
beam. A x-50 attenuator was in the
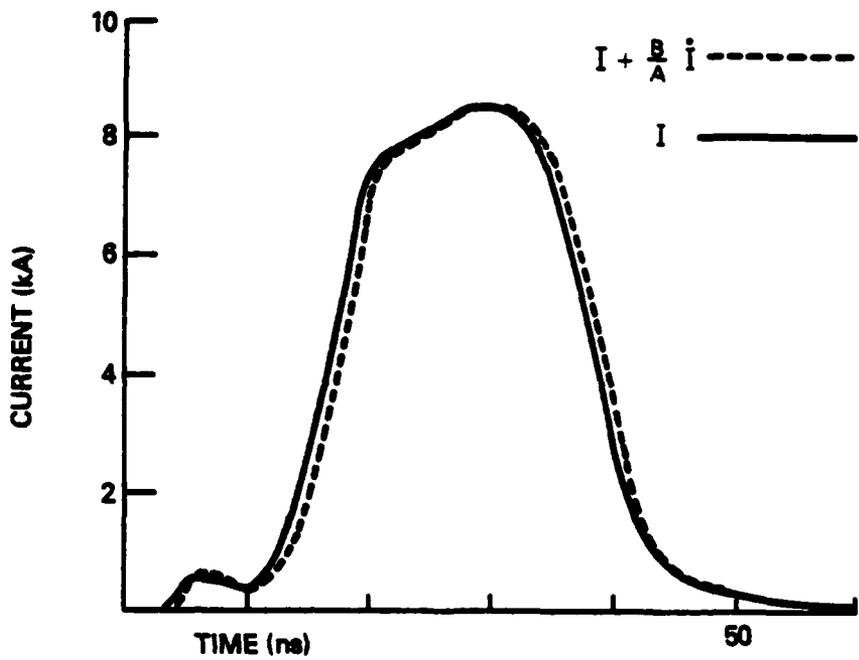probe cable.

Fig. 11 — A "beam bug" record of the total beam current (solid line) and a hypothetical probe signal (dotted line) for a beam without hose-like or sausage-like perturbations
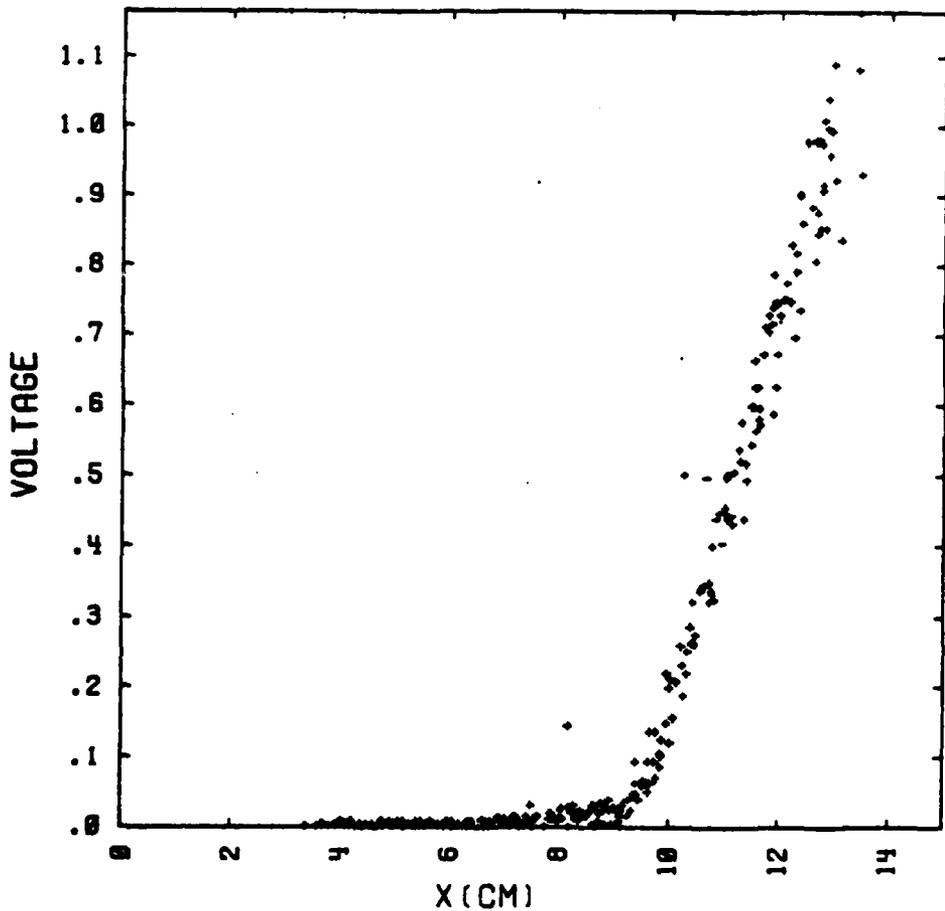

Fig. 12 — Probe voltage versus depth of insertion. The data is for a time of 28 ns. A x-50 attenuator was in the probe cable.
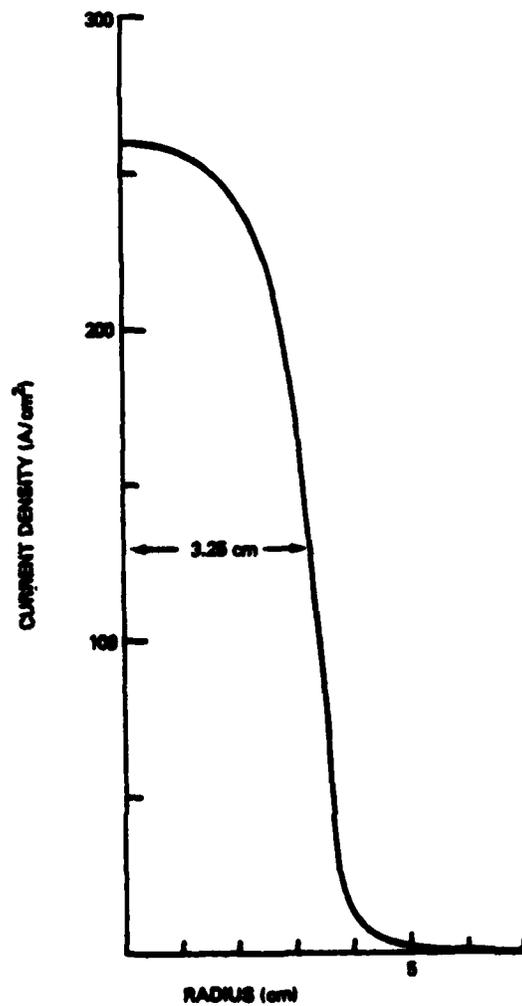
15

Fig. 13 — The beam current profile at 28 ns as determined from Fig. 12 and the theoretical probe calibration
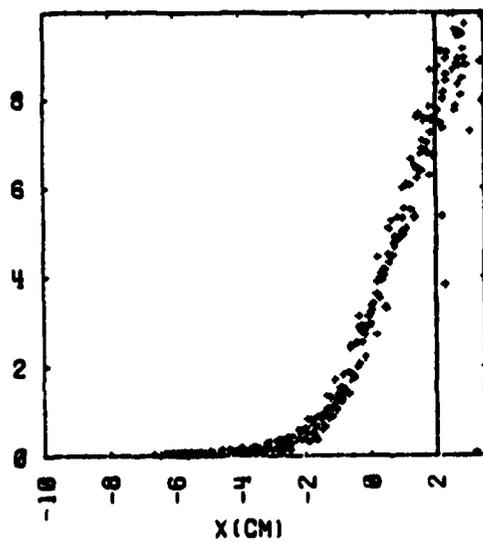

Fig. 14 — Probe voltage summed over time versus depth of insertion. An ordinate of 1 corresponds to 1.56×10^{-7} volt-sec. The zero position of the abscissa is arbitrary. The vertical line represents the position of the probe tip when the nonuniform base of the probe begins to enter the beam.

16

Fig. 15 — The time integrated beam profile as
determined from Fig. 14 and the theoretical
probe calibration

CHARGE DENSITY (MICROCOULOMBS/cm²)
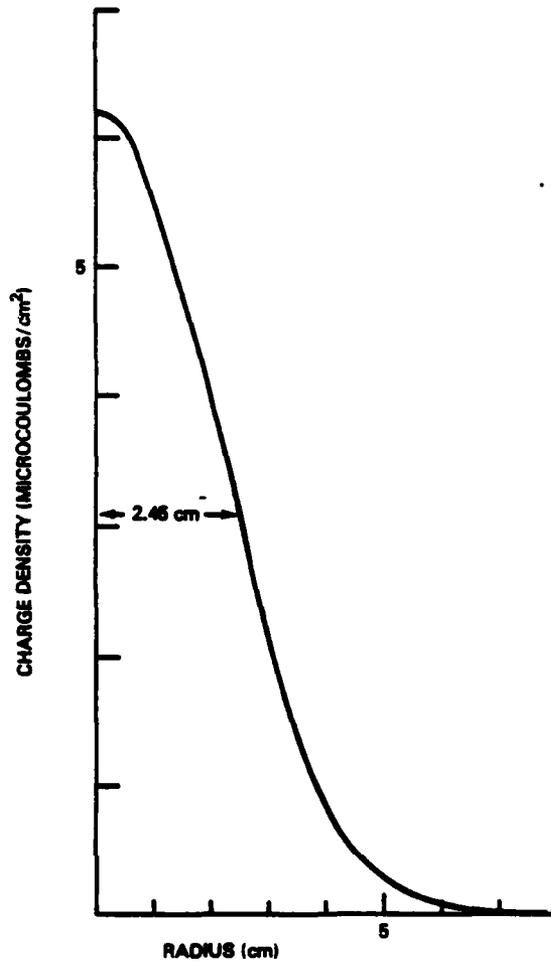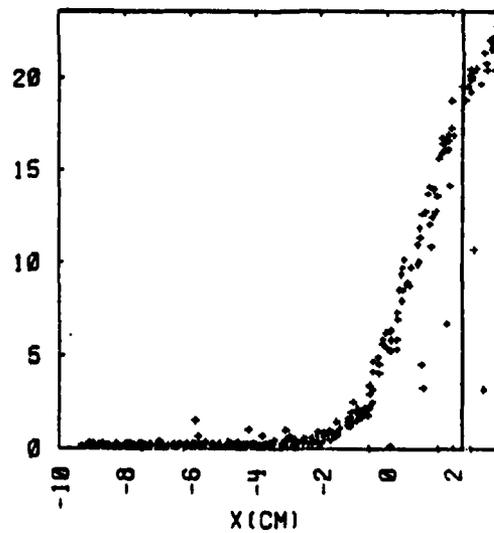
← 2.46 cm →

5

RADIUS (cm)

Fig. 16 — The x-ray probe signal, summed over
time, versus depth of insertion. The vertical line
represents the position of the probe tip when the
nonuniform base of the probe begins to enter the
beam. The zero position is arbitrary.

20

15

10

5

0

X (CM)

17